Research Article

Nouf Omar Alafaleq, Alya Alomari, Mohd Shahnawaz Khan*, Gouse M. Shaik, Afzal Hussain, Faheem Ahmed, Iftekhar Hassan, Ibrahim M. Alhazza, Majed S. Alokail, Amal Majed H. Alenad, Nasimudeen R. Jabir, and Shams Tabrez*

Anticancer potential of gold nanoparticles (AuNPs) using a battery of *in vitro* tests

https://doi.org/10.1515/ntrev-2022-0502
received May 23, 2022; accepted November 28, 2022

Abstract: This study synthesized gold nanoparticles (AuNPs) using a facile microwave-assisted chemical route and evaluated them as potential anticancer candidates against breast and colon cancer cell lines. Numerous spectral characterization tools were used to study the optical properties, structure, and morphology of the prepared AuNPs. UV-Vis spectroscopy showed a characteristic peak at 517 nm, which confirms the formation of AuNPs. The crystalline structure of NPs was studied by X-ray diffraction, and the NPs' shape and size were calculated with Field emission transmission electron microscopy. The synthesized AuNPs were found to be uniform in size in the range of 2–6 nm. A variety of biological tests, including MTT, scratch, real time polymerase chain reaction (RT-PCR), and comet assays were adopted to assess the anticancer potential of these AuNPs in the studied cancer cell models. The findings suggested a cell-dependent cytotoxicity of AuNPs. Different cell viability of 40.3 and 66.4% were obtained for MCF-7 and HCT-116, respectively, at 5 μg/mL of AuNPs. The scratch assay showed AuNPs impede cell migration in a concentration-dependent manner in the MCF-7 cell line. On the other hand, real-time polymerase chain reaction (RT-PCR) of apoptotic (p53, Bax, and caspase-3) and anti-apoptotic (BCl-2) genes revealed upregulation and downregulation of these genes, respectively, probably leading to its cytotoxicity. At 5 μg/mL concentration of AuNPs, reactive oxygen species (ROS) production was found to be increased by 26.4 and 42.7%, respectively, in MCF-7 and HCT-116 cells. Similarly, comet assay demonstrated AuNPs induced DNA damage in the studied cancer cell lines. These findings suggest that the observed anticancer efficacy of AuNPs was driven by ROS generation. The synthesized AuNPs appeared to be a promising therapeutic against cancer cells. However, our *in vitro* data need to be confirmed and validated in *ex vivo* and *in vivo* models so that this NP can be further exploited for human use.

Keywords: cytotoxicity, gold nanoparticles, ROS, RT-PCR, scratch assay

*** Corresponding author: Mohd Shahnawaz Khan,** Department of Biochemistry, College of Science, King Saud University, Riyadh, Saudi Arabia, e-mail: moskhan@ksu.edu.sa
*** Corresponding author: Shams Tabrez,** King Fahd Medical Research Center, King Abdulaziz University, Jeddah, Saudi Arabia; Department of Medical Laboratory Science, Faculty of Applied Medical Sciences, King Abdulaziz University, Jeddah, Saudi Arabia, e-mail: shamstabrez1@gmail.com
Nouf Omar Alafaleq, Alya Alomari, Gouse M. Shaik, Majed S. Alokail, Amal Majed H. Alenad: Department of Biochemistry, College of Science, King Saud University, Riyadh, Saudi Arabia
Afzal Hussain: Department of Pharmacognosy, College of Pharmacy, King Saud University, Riyadh, Saudi Arabia
Faheem Ahmed: Department of Physics, College of Science, King Faisal University, P.O. Box 400, Al-Ahsa 31982, Saudi Arabia
Iftekhar Hassan: Department of Zoology, College of Science, King Saud University, Riyadh, Saudi Arabia, e-mail: ihassan@ksu.edu.sa
Ibrahim M. Alhazza: Department of Zoology, College of Science, King Saud University, Riyadh, Saudi Arabia, e-mail: ihazza@ksu.edu.sa
Nasimudeen R. Jabir: Department of Biochemistry, Centre for Research and Development, PRIST University, Vallam, Thanjavur, Tamil Nadu, India

1 Introduction

Cancer is one of the most clinically relevant pathologies driven by highly heterogeneous processes and has remained a major public health concern worldwide [1–3]. Among the various types of cancer, breast and colorectal cancer have significant occurrence, expression, and mortality. Breast cancer is the most frequently diagnosed and the leading cause of cancer death in women worldwide, with more than 2 million new cases in 2020 [4,5]. Conversely, colorectal cancer is the third most prevalent cancer in men and the second most common cancer in women worldwide [6,7].

Despite the potential advances in anticancer research, limited progress has been made toward the safe treatment and prognosis of cancer [8]. The escalating complexity of the cancer problem, combined with the inability of

traditional chemotherapy to achieve significant reductions in mortality rates, indicates the requirement of noble, harmless, yet concrete chemotherapeutic approaches to impede cancer progression. Nanotechnology can be pivotal in cancer treatment and prevention [9,10]. The nanoparticles (NPs) can be modulated to prolong circulation, improve drug localization and efficacy, and reduce the chances of multi-drug resistance [11,12].

Over the past few years, precision-engineered nanomaterials have risen as a standout among cancer therapeutics with a tremendous anticancer therapeutic perspective [13,14]. They can improve the delivery of therapeutics to the specific sites of the body at particular times and at an effective concentration. Several reports suggested different therapeutic benefits of NP-based treatment that could act as molecular probes, antiangiogenic, antitumor, anti-permeability, and antiproliferative [2,15–17].

Among nanotherapeutics, gold nanoparticles (AuNPs) have attracted extensive scientific attention in recent decades because of their convenience of synthesis. AuNPs are increasingly used in medicine because of their excellent biocompatibility due to their chemical and physical stability and ease of functionalization with biologically active molecules [18]. AuNPs can directly conjugate and interact with a wide range of molecules on their surface, including proteins, medicines, antibodies, enzymes, nucleic acids (DNA or RNA), and fluorescent dyes [19]. AuNPs are qualified as efficient nanomedicine with potent anticancer activity due to their unique physicochemical and bio-reactive properties [20]. Distinctive properties of AuNPs, *viz*., high X-ray absorption coefficient, localized surface plasmon resonance, and radioactivity, enable its prominent clinical applications [21]. AuNPs can serve as molecular sensors, therapeutics, and delivery systems for imaging agents and medications [22]. Functionalized AuNPs have made significant strides as they have the potential for effective cellular uptake. However, other factors, such as the nature of the ligand, molecular weight, and grafting density, also affect the cellular uptake [23]. Along with other factors like size, cell type, tissue distribution, tissue absorption, and penetrating ability, AuNPs-induced cytotoxicity is also influenced by these [24]. Due to the impact of surface energy transfer, AuNPs are a potent quencher for fluorescence donors, making them an ideal building block for fluorescent nanoprobes [22]. Although no pharmaceutical approval of AuNPs has been achieved, several studies suggested their usage in cancer therapy and tumor-targeting [25–27].

Our earlier study reported the anti-metastasis potential of biogenic synthesized AgNPs against breast and colorectal cancer cells and suggested it as a promising anticancer therapy [2]. In the current study, the anticancer potential of the synthesized AuNPs was assessed employing a battery of *in vitro* tests, including cell viability, cell morphology, cell migration, reactive oxygen species (ROS) production, DNA damage, modulation in pro/anti-apoptotic gene expression, and induction of apoptosis.

2 Materials and methods

2.1 Materials

Cell lines (MCF-7 and HCT-116) were obtained from ATCC (Manassas, VA, USA). Chloroauric acid ($HAuCl_4$), citric acid, and cetyltrimethylammonium bromide (CTAB), 3-(4,5-dimethylthiazol-2-yl)-2,5-diphenyltetrazoliumbromide (MTT), 2,7 dichlorofluorescin diacetate (DCFH-DA), Dulbecco's modified Eagle's medium (DMEM) high glucose, Fetal bovine serum (FBS), and penicillin were obtained from Sigma-Aldrich (St. Louis, MO, USA). All other chemicals used for this study were of the highest purity grade and procured from different commercial sources.

2.2 Preparation of AuNPs

To synthesize AuNPs, a solution containing 15 mL of 10 mM $HAuCl_4{\cdot}3H_2O$, 0.3 g citric acid, and 0.2 g CTAB were mixed under continuous stirring to obtain an aqueous solution. This solution was then heated for 50 s at 100 W in a microwave oven (SAMSUNG; 750 W), resulting in an immediate shift in color from light yellow to bright orange, indicating the formation of gold NPs. The AuNPs were extracted from the solution using the Whatman qualitative filter paper of grade 1.

2.3 Characterization of AuNPs

A UV-Vis Spectrophotometer (Perkin Elmer, USA) with a 1 cm quartz cell was used to characterize the synthesized AuNPs. In a quartz cell, colloidal AuNPs were mixed with 5 mL of distilled water, and the blank was filled with a distilled water solution. The crystalline structure of the synthesized NPs was studied using X-ray diffraction (Philips-PW 1729, Holland) with Cu radiation [30 kV, 40 mA, Kα radiation (1.54430 A°)]. In addition, field emission transmission electron microscopy (FETEM; JEOL, JEM-2100F) at 200 keV was used to examine the NPs'

shape and size. A small drop of NP solution was dropped onto a carbon-coated copper grid, which was then dried in the air before being transferred to the microscope. "Image J" program was used to determine the NP's average particle size and distribution.

2.4 Cytotoxicity/MTT assay

3-(4,5-Dimethylthiazol-2-yl)-2,5-diphenyltetrazolium (MTT) bromide dye reduction test was used to determine the cytotoxicity of AuNPs, as described previously [2,28]. Briefly, MCF-7 and HCT-116 cells (10,000 cells/well) were seeded on 96-well culture plates and treated with variable concentrations of AuNPs (0.5–100 μg/mL) for 24 h and kept in CO_2 incubator. Following the incubation period, 10 μL of MTT (5 mg/mL stock in PBS) was added to each well, and the plates were further incubated at 37°C for 4 h. The formazan product was then dissolved in 100 μL of dimethyl sulfoxide (DMSO) with moderate shaking at 37°C. and the absorbance was recorded at 570 nm on a microplate reader (Chameleon-Multilabel microplate reader, Hidex, Turku, Finland).

2.5 Cell migration (scratch assay)

To assess the anti-metastasis ability of AuNPs, we performed an *in vitro* scratch assay following the protocol described by Khan *et al.* [2]. Briefly, MCF-7 cells were seeded in a 24-well cell culture plate and incubated for 24 h. Once monolayers of MCF-7 cells were grown to confluency, a thin scratch was introduced with a sterile tip, and cells were briefly washed with DMEM to decant any detached cells. After the scratch was introduced, cells monolayer was incubated with control and varying concentrations of AuNPs (1–4 μg/mL). Pictures of scratch were taken every 24 h up to 48 h at 10× magnification of Leica DFC 450 microscope equipped with a camera. The pictures were processed using Image J software and aligned with control.

2.6 Comet assay

The assay was carried out according to method adopted and modified by Hassan *et al.* [29]. The full-grown cells were treated with AuNPs (5 μg/mL) for 3 h in Petri-dishes. The cells were then trypsinized to prepare the cell suspension and homogenized in 1 mL of media. The cells were then centrifuged for 5 min at 500 g. An equal volume of cell suspension (100 μL) was mixed with 1% low melting agarose (100 μL). This solution was placed on conventional melting agarose base-coated slides. For 10 min, the slides were immersed in lysis buffer (0.045 M TBE, pH 8.4, containing 2.5% SDS). After that, the slides were exposed to the same TBE buffer without SDS in a comet assay tank for 10 min at 2 V/cm and 80 mA, respectively. Finally, the cells were stained with ethidium bromide (20 g/mL, Sigma-Aldrich, USA). After proper washing, the slides were covered with coverslips and preserved in a humidified environment. 100 cells from each group were examined using an upright fluorescence microscope (Leica DM2500, Germany) equipped with a digital CCD camera to measure the tail length of nuclear DNA (Andor Zyla 5.5, UK). Komet 5.5 image analysis software was used to measure and picture the tail length (Andor, UK).

2.7 ROS measurement

DCFH-DA was used to detect the intracellular generation of ROS [17,30]. The extremely fluorescent chemical DCF is formed when the DCFH-DA reacts with ROS after passively entering the cell. In 24-well plates, cancer cells (5×10^4 cells/well) were seeded and left to adhere to the flask for 24 h. It was then exposed to various concentrations of AuNPs (1–10 μg/mL) and incubated for an additional 24 h. After exposure, the cells underwent two PBS washes before being incubated for 30 min at 37°C in 1 mL of the working solution of DCFH-DA (100 μM). After 10 min of centrifugation, 200 μL of the cell supernatant was transferred to a 96-well plate. The fluorescence intensity was measured at wavelengths of 485 nm for excitation and 525 nm for emission.

2.8 Gene expression analysis (Real time-PCR)

MCF-7 and HCT-116 cells were grown to confluency in 6-well plates and treated with AuNPs (5 μg/mL) for 24 h. Appropriate control cells were also treated with PBS. These cells were further subjected to RNA extraction using the RNeasy mini kit (Qiagen, Germany). The concentration and purity of total RNA were confirmed by a Nanodrop spectrophotometer (Thermo Scientific, USA). A total of 1 μg of RNA was used to synthesize the cDNA using 100 ng of oligo dTs and 2 units of reverse transcriptase. The following sets of specific primers were employed for amplification of each cDNA: p53 (5′F-CCCAGCCAAAGA AGAAACCA-3′, 5′R-TTCCAAGGCCTCATTCAGCT-3′), caspase3 (5′F-ACATGGCGTGTCATAAAATACC-3′, 5′R-CACAAAGCGA

CTGGATGAAC-3′), Bax (5′F-TGCTTCAGGGTTTCATCCAG-3′, 5′R-GGCGGCAATCATCCTCTG-3′), Bcl2 (5′F-AGGAAGTGAAC ATTTCGGTGAC-3′, 5′R-GCTCAGTTCCAGGACCAGGC-3′), and GAPDH (5′F-CCACTCCTCCACCTTTGAC-3′, 5′R-ACCCTGTTGC TGTAGCCA-3′). Real-time quantification was performed in the light of Cycler® 480 instrument with 96-well plate (Roche Diagnostics, Rotkreuz, Switzerland) using Light Cycler® 480 SYBR Green I Master (Roche Diagnostics, Switzerland). The RT-PCR cycle conditions were 10 min of initial denaturation at 95°C, followed by 40 cycles of denaturation at 95°C for 15 s, annealing at 60°C for 20 s, and elongation at 72°C for 20 s. Gene expression levels were normalized to GAPDH gene expression, which was used as an internal housekeeping control.

2.9 Flow cytometry

The induction of apoptosis as a result of AuNPs treatment was measured using a Flow cytometer (BD FACSCalibur®, USA) following the method demonstrated by Hailan *et al.* [31]. A commercially available FITC-Annexin V apoptosis detection kit supplied by BD Pharmingen™, (CA, USA) was employed. Briefly, the cancer cells (MCF-7 and HCT-116) were grown to confluency and further exposed to the different concentrations of AuNPs (2 and 5 µg/mL) for 24 h. After that, cells were resuspended in 1× binding buffer and treated for 20 min in the dark with annexin V-FITC and propidium iodide (5 µL each). A flow cytometer was used to quickly analyze each sample, and Cell Quest® Pro software was used to analyze the results (BD).

2.10 Statistical analysis

The results of each experiment were provided as the average of three independent replicates ± standard error. Unless otherwise specified in the legends, the student's *t*-test was used to analyze the difference between the control and test groups.

3 Results

3.1 Synthesis and characterization of AuNPs

Citric acid was used as a reducing agent and CTAB as a binding agent during microwave irradiation. After 50 s of irradiation, the produced AuNPs were discovered to be stable and to have a size range of 2–6 nm. The UV-Vis absorption spectra of AuNPs showed the surface plasmon resonance peak at ~517 nm, confirming the AuNP synthesis (Figure 1a). The size of the NPs can be determined with accuracy by the peak's width. The peak narrows with the decrease in bandwidth and increase in the band strength as the particle size increases [32]. The size, shape, and dielectric constant of the surrounding media all affect the form and location of surface plasmon absorption. The optical absorption spectra of metal NPs are mostly determined by the surface plasmon resonance, which moves to a longer wavelength as particle size increases.

The detailed morphology of AuNPs was investigated by high-resolution transmission electron microscopy (HRTEM) and TEM at room temperature. The TEM images showed stable, well-dispersed, spherical AuNPs with good morphological characteristics (Figure 1b). In addition, TEM measurements also indicated that the obtained material consists of uniform populations of NPs. Particle size was calculated using approximately 50 randomly selected individual NPs from TEM micrographs, and found the particle size was in the 2–6 nm diameter range (Figure 1c). TEM images also showed an essential role played by CTAB in stabilizing the AuNPs. Structural information of AuNPs was further analyzed by HRTEM image. The inset of Figure 1b shows the HRTEM image of a single AuNP, where clear lattice fringes could be easily seen. The distance between two adjacent planes was found to be 0.236 nm, which is linked with (111) plane of Au structure.

XRD pattern analysis was used to assess the crystal structure and phase determinations of the produced NPs. The XRD pattern of AuNPs, displaying the diffraction peaks of AuNPs, is shown in Figure 1d. The (1 1 1), (2 0 0), and (2 2 0) reflections of the face-centered cubic structure of metallic gold, respectively, can be indexed to the peaks located at 38.16, 44.47, and 64.63° [33]. The peak corresponding to (1 1 1) was also found to be more intense than the other peaks, indicating that this orientation is the most common and that the produced AuNPs are naturally crystalline. Within the XRD's detection range, no additional phase was found. In addition, the average crystal size of AuNPs was calculated using the Debye–Scherrer's equation by determining the width (111) of the Bragg's reflection was found to be 5.8 nm.

3.2 Anticancer activity of AuNPs: MTT, scratch, and comet assay

After establishing the purity of the synthesized AuNPs, a battery of *in vitro* experiments was performed to evaluate the biological efficacy of AuNPs. The synthesized NPs

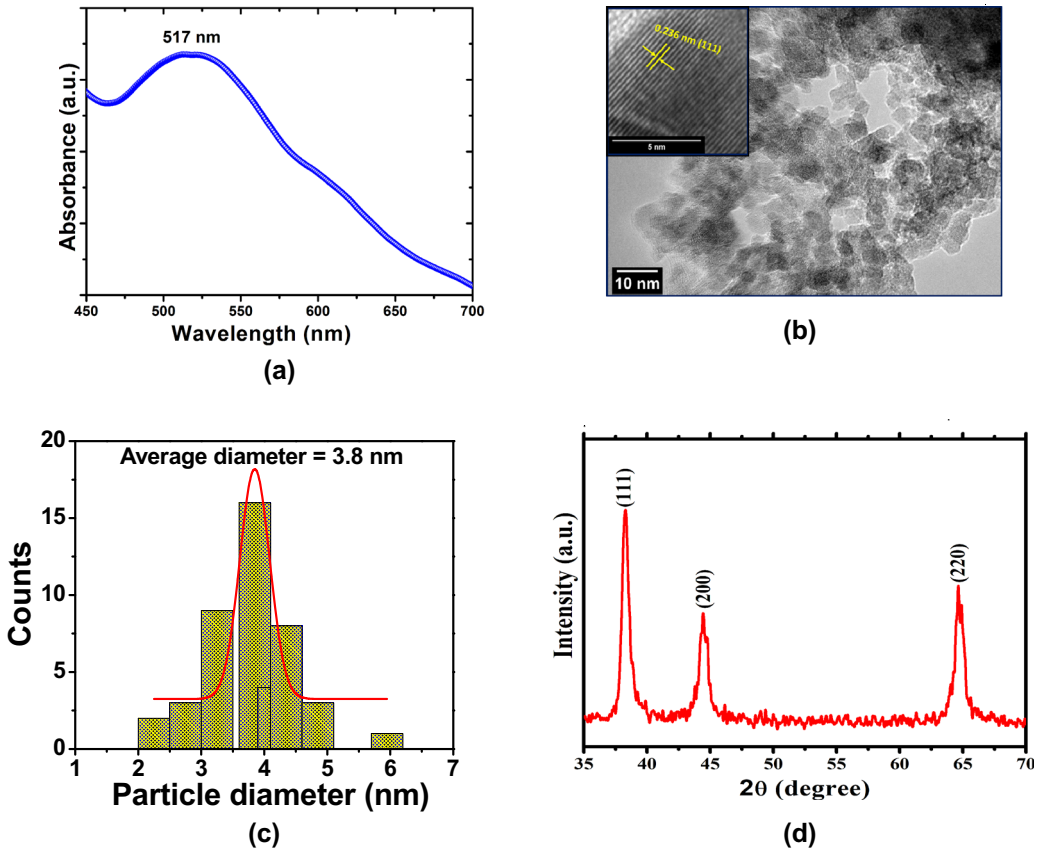

Figure 1: (a) UV-Vis spectrum of AuNPs synthesized at 50 s MWI. (b) TEM image and inset show HRTEM image of AuNPs synthesized at 50 s MWI. (c) Size distribution histogram obtained from TEM images of AuNPs. (d) XRD pattern of AuNPs synthesized at 50 s MWI.

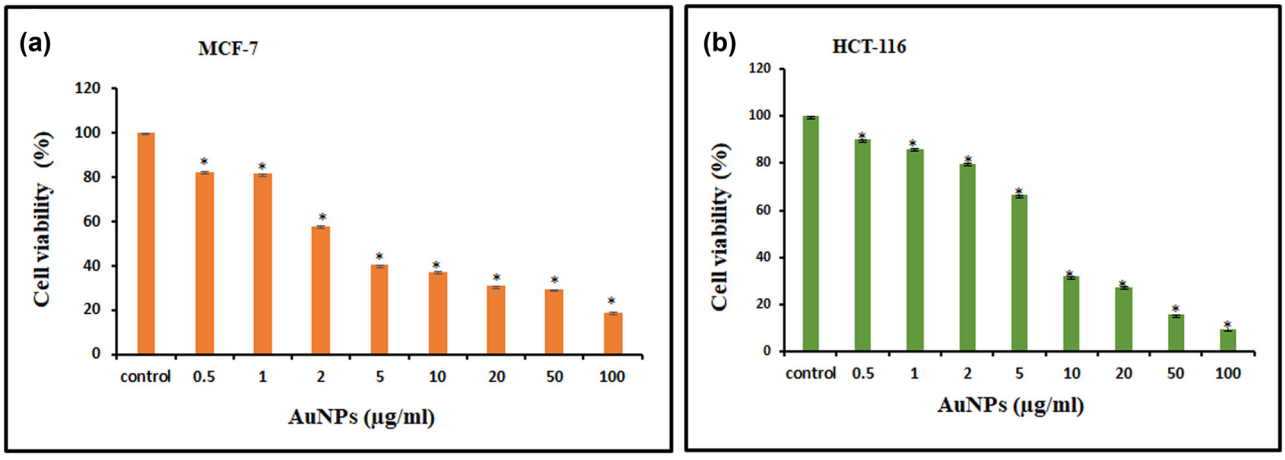

Figure 2: MTT-based cell viability assay. For 24 h, cells were treated with varying concentrations of AuNPs (0.5–100 µg/mL). For both MCF-7 (a) and HCT-116 (b) cell lines, results are reported as column graph with normalized percent cell viability with standard deviation. Data are the mean value ± SD of three independent experiments. Student *t*-test was performed to determine the significance. *P*-values < 0.05 (compared to control) were considered a significant criterion and indicated with * mark over the column.

were found to be cytotoxic in a concentration-dependent manner to MCF-7 and HCT-116 cell lines. Different cell viability of 40.3 and 66.4% were obtained for MCF-7 and HCT-116, respectively, at 5 µg/mL of AuNPs (Figure 2a and b). The percentage of cell viability was found to be declined even at a very low concentration (0.5 µg/mL) of AuNPs, suggesting its high toxicity toward cancer cells. On the other hand, the morphology of the cancer cells

was also found to be notably distorted in both cell lines with increase in the concentration of AuNPs treatment for 24 h (Figure 3). Scratch assays examined the cancer cell migration and invasion in the presence of AuNPs. The data showed a significant suppression in wound healing and cell migration following the treatment with 2 µg/mL of AuNPs in MCF-7 cells after 48 h of incubation compared to control (Figure 4). Less migration was observed at higher concentrations of AuNPs, which was also found to be variable with time. Because HCT-116 cells develop in bunches, we were unable to measure their migration pattern (data not shown).

3.3 AuNPs-induced DNA damage in MCF-7 and HCT-116 cells

The present study used a comet assay to evaluate the DNA damage induced by AuNPs, resulting in a combination of single-strand breaks, double-strand breaks, and alkaline-labile sites. In this experiment, negatively charged DNA fragments move towards the positive electrode, whereas the broken DNA fragments move towards the positive electrode by carrying a negative charge. At the same time, the unbroken DNA stays intact without any movement. The untreated control cells showed an intact round-shaped nucleus without a noticeable tail comet-like structure. However, the treatment with AuNPs (5 µg/mL) showed a significant damage to the nuclear DNA of MCF-7 and HCT-116 cells, reflected by a longer tail length (Figure 5). The comet tail was found to be increased by 56% compared to the untreated control in MCF-7 cells. Similarly, the comet tail in the HCT-116 cell was found to be increased by 62% compared to the untreated control.

3.4 AuNPs-induced intracellular ROS generation in MCF-7 and HCT-116 cell lines

We evaluated the intracellular ROS level by measuring DCF fluorescence. The DCF fluorescence was assessed in AuNPs-treated cancer cells at 1–10 µg/mL doses for 24 h. A dose-dependent increase in ROS production was observed after the treatment with AuNPs in both the studied cell lines. We observed a considerable increase (26.4%) in ROS generation in MCF-7 cells compared to control at 5 µg/mL of AuNPs. Similarly, HCT-116 cells also showed an increase (42.7%) in ROS generation after the treatment with the same concentration of AuNPs (Figure 6). Our results showed significant ROS-producing capabilities of AuNPs in MCF-7 and HCT-116 cell lines (Figure 6).

3.5 Effect of AuNPs on mRNA expression of pro/anti-apoptotic marker genes in MCF-7 and HCT-116 cancer cells

The treatment with 5 µg/mL AuNPs showed increased expression of tumor suppressor gene p53 and elevated expression of pro-apoptotic genes, Bax, and caspase-3. On the other hand, the expression of the anti-apoptotic gene BCL-2 was found to be downregulated in MCF-7 cells

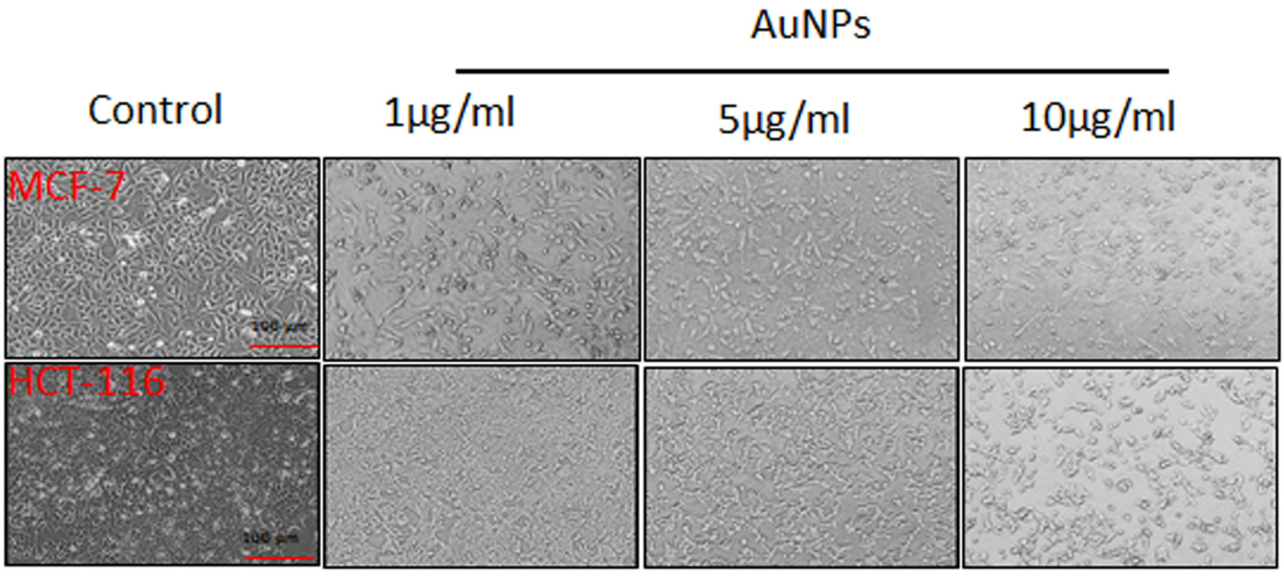

Figure 3: MCF-7 and HCT-116 cells were treated with increasing concentrations of AuNPs for 24 h and showed morphological alterations. The images were captured using a Leica microscope at 10× magnification.

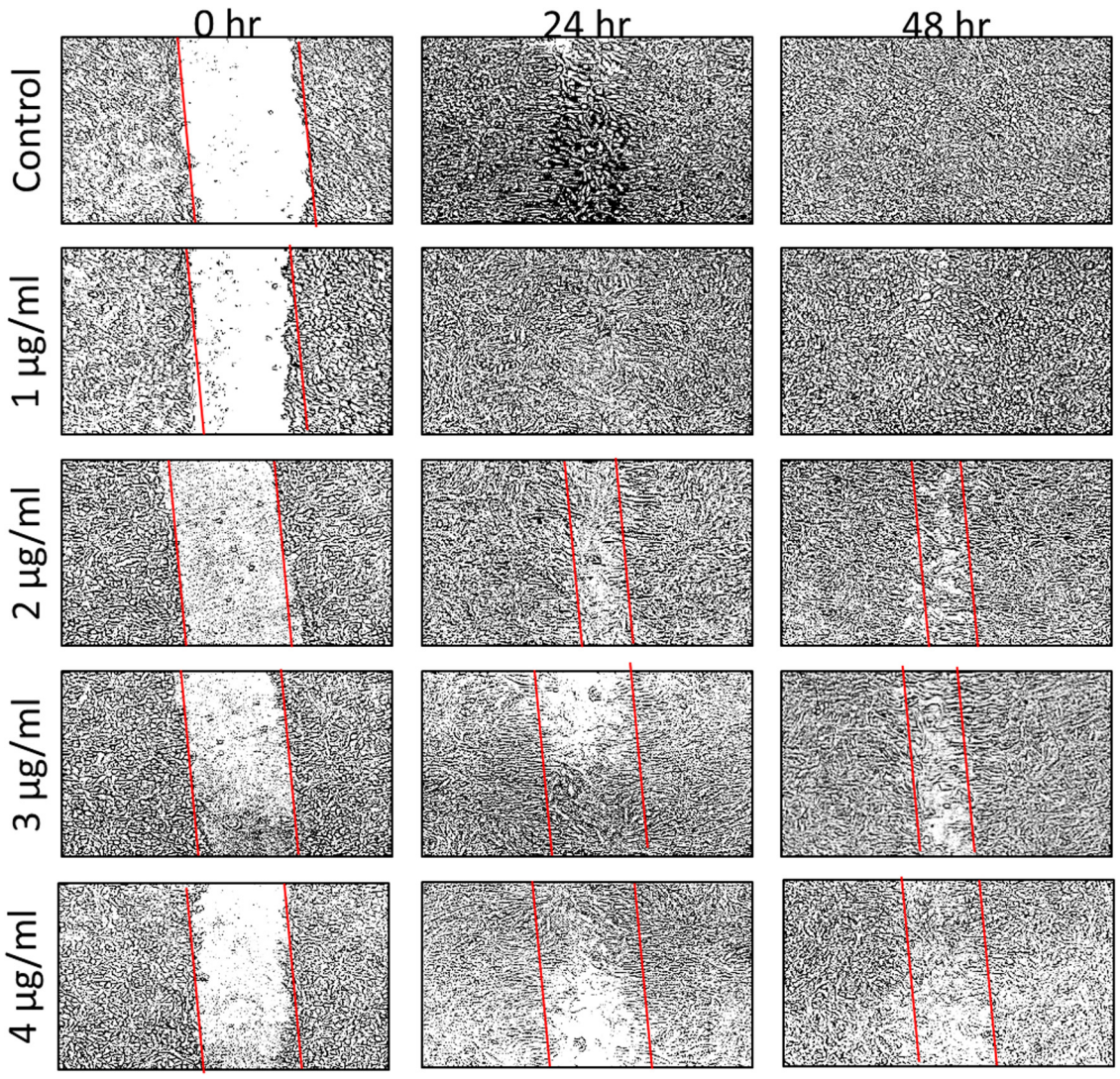

Figure 4: Scratch was applied to a monolayer of cells, which was then treated with 1–4 µg/mL AuNPs at various time intervals (0, 24, and 48 h). The number of cells that migrated to the scratch area, indicating metastatic inhibition, is visually displayed by outlining the scratch with parallel lines and visually exhibiting the number of cells that migrated to the scratch area.

(Figure 7a). A similar trend was also recorded in HCT-116 cells at the same concentration of AuNPs (Figure 7b).

3.6 Induction of apoptosis by AuNPs in MCF-7 and HCT-116 cells

The results of the apoptosis quantification in MCF-7 and HCT-116 cells are presented in dot plots (Figures 8a and b; 9a and b). Both the cells experienced a significant increase in apoptosis in a dose-dependent manner. At 2 µg/mL, the rates of early apoptosis were 15.59 and 12.32%, respectively, for MCF-7 and HCT-116 cells. At the same time, the levels of late apoptosis were 10.69 and 13.19% at the same concentration. Similarly, the highest concentration of AuNPs (5 µg/mL) treatment showed 18.78 and 18.92% early apoptotic cells in MCF-7 and HCT-116 cell lines. In addition, the treatment of AuNPs resulted in a slight elevation in necrotic cells in a concentration-independent manner. Conclusively, apoptosis analysis reaffirms the cytotoxicity data of cancer cells towards AuNPs.

4 Discussion

The growing body of evidence indicates that NPs are up-and-coming candidates for drug delivery as an adjuvant to existing treatment or a possible therapeutic agent for

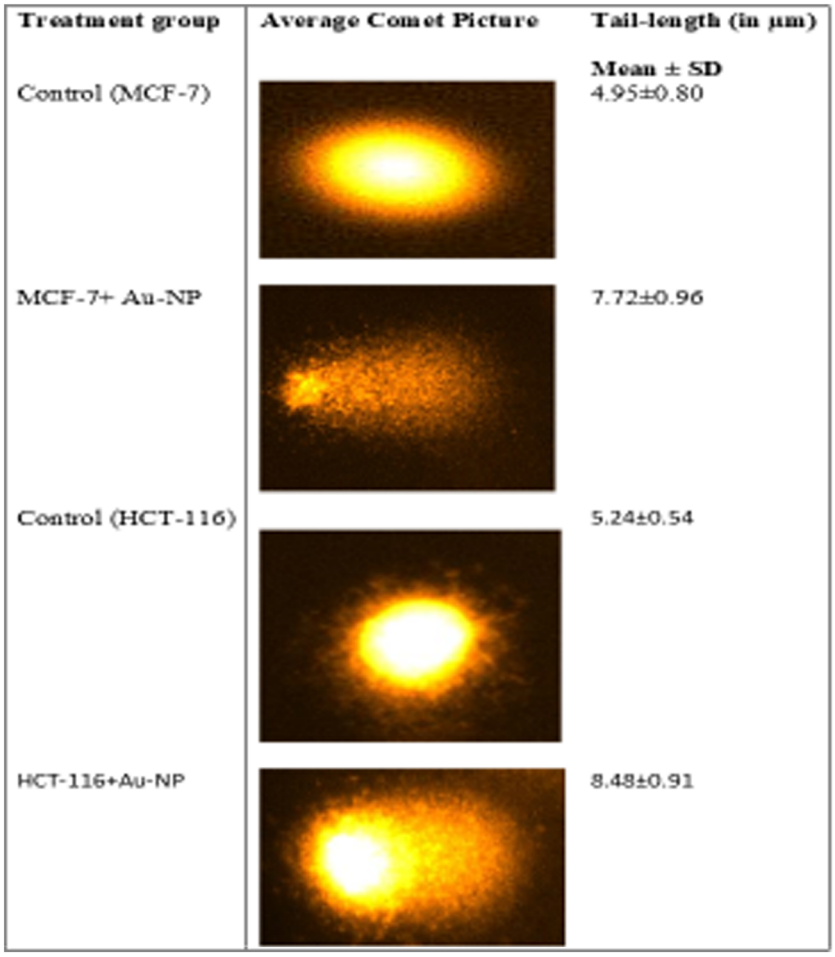

Figure 5: Comet assay was used to evaluate the DNA damage caused by AuNPs (5 µg/mL) in the studied cancer cells. The results showed a significant DNA damage caused by AuNPs treatment, as observed by increase in the tail length of DNA in cancer cells.

various disorders, including cancer [34–36]. The current study exploited the microwave irradiation technique with citric acid as a reducing agent to synthesize AuNPs, while multi-technique approaches were adopted for the characterization purpose. The synthesized AuNPs were stable and ranged between 2 and 6 nm for 50 s irradiation time. In recent years, the microwave irradiation (MWI) approach has emerged as a new strategy to synthesize smaller size AuNPs rapidly [37,38]. The method allows the regulation of AuNP properties and structure, while avoiding contamination by altering experimental conditions in the presence of a reducing agent [19]. Recently, Adnan *et al.* [25] reported a microwave-assisted synchronous nanogold synthesis with superior characteristics in terms of high-quality crystal, spherical shape, amorphous, enhanced colloidal stability, and no agglomeration with feasible biocompatibility, biosafety, and anticancer therapeutic value. The specific size and configuration of AuNPs greatly affect the anticancer potential, including cytotoxicity [39]. Despite favorable results with smaller size AuNPs, the very low size could result in rapid excretion through the renal filtration system [40,41]. In one study, Zhang *et al.* [24] reported that smaller AuNPs (4–5 nm) have a higher cytotoxicity potential compared to larger particles (18–20 nm). Hence, our synthesized AuNPs (2–6 nm) are expected to provide an optimum anticancer therapeutic effect.

The cytotoxicity of AuNPs has been reported in many cancer cell lines, such as Hep2, MDA-MB-231, Caco-2, and MCF-7 cancer cells [27,42,43]. The cytotoxicity of AuNPs is associated with NP size, surface charge, and functional groups [44]. The smaller size of AuNPs results in extensive tissue distribution, deep penetration inside specific tissues, better cellular uptake, and increased toxic effects [45]. Considering the abovementioned facts, we observed significant cytotoxicity of the synthesized AuNPs at very low concentrations in both the cell lines. The smaller size and varied surface characteristics of AuNPs could be the reason behind the observed significant cytotoxicity.

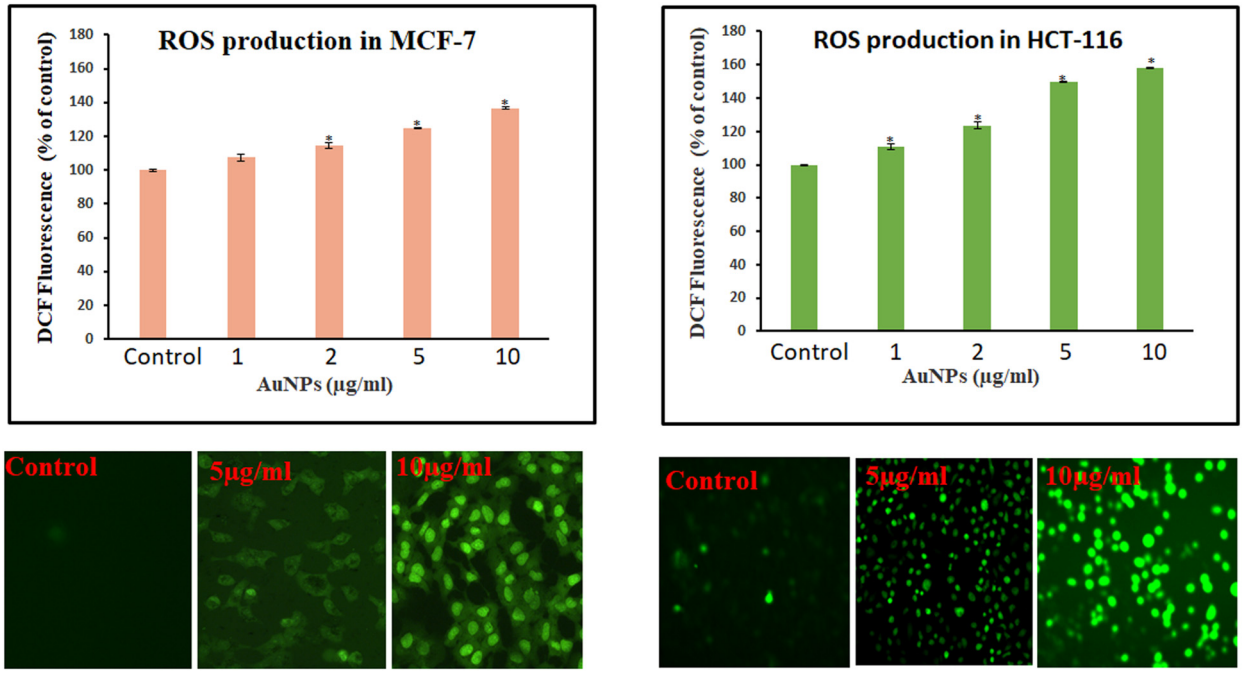

Figure 6: ROS production in MCF-7 and HCT-116 cells treated with AuNPs. A spectrofluorometer was used to detect the relative fluorescence of DCF, with excitation and emission spectra of 485 and 530 nm, respectively. Student *t*-test was performed to determine the significance. Values <0.05 were considered significant and indicated with * mark above the column. A Leica microscope (20× magnification) was used to take the image of the fluorescing cells.

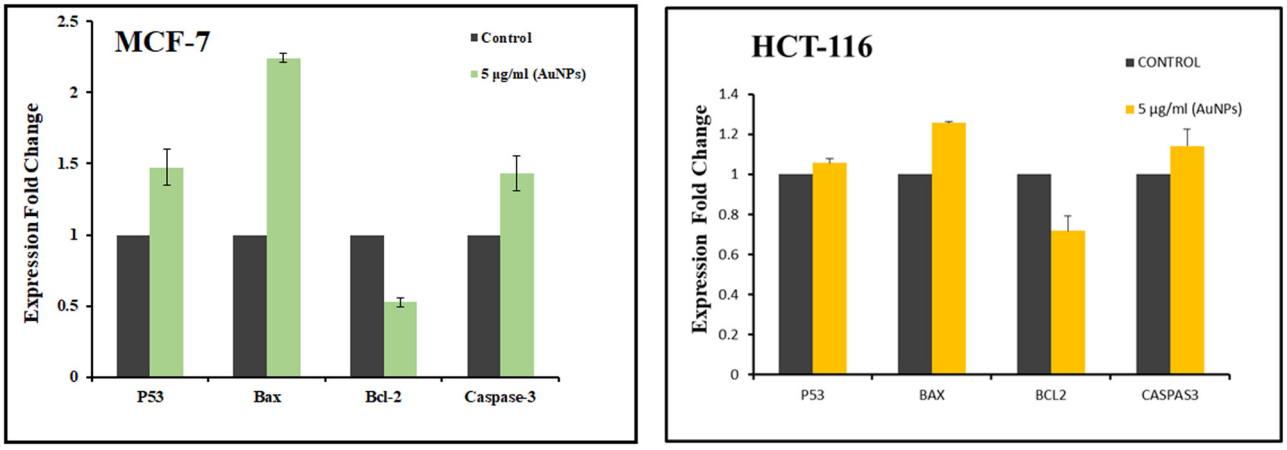

Figure 7: Effect of AuNPs on pro/anti-apoptotic marker mRNA expression levels. Changes in mRNA expression levels caused by nanostructures are expressed as a fold change in relative quantity compared to control cells. Other genes' cycle threshold values were computed using GAPDH as a control.

The migration of cells is crucial for the progression of cancer. In this study, we used an *in vitro* scratch assay since it is a reliable tool for probing cell migration [46]. The potential of AuNPs to interfere with the cytoskeleton of MCF-7 cells may explain the suppression of migration observed in our study. Cell division and migration necessitate cytoskeleton rearrangement and disrupting one or both processes significantly impacts cell proliferation and migration [47]. Our findings are consistent with earlier studies that reported NPs limit cancer cell migration [26,48].

For the quantitative measurement of DNA damage, the comet assay assessing a mixture of single-strand breaks, double-strand breaks, and alkaline-labile sites

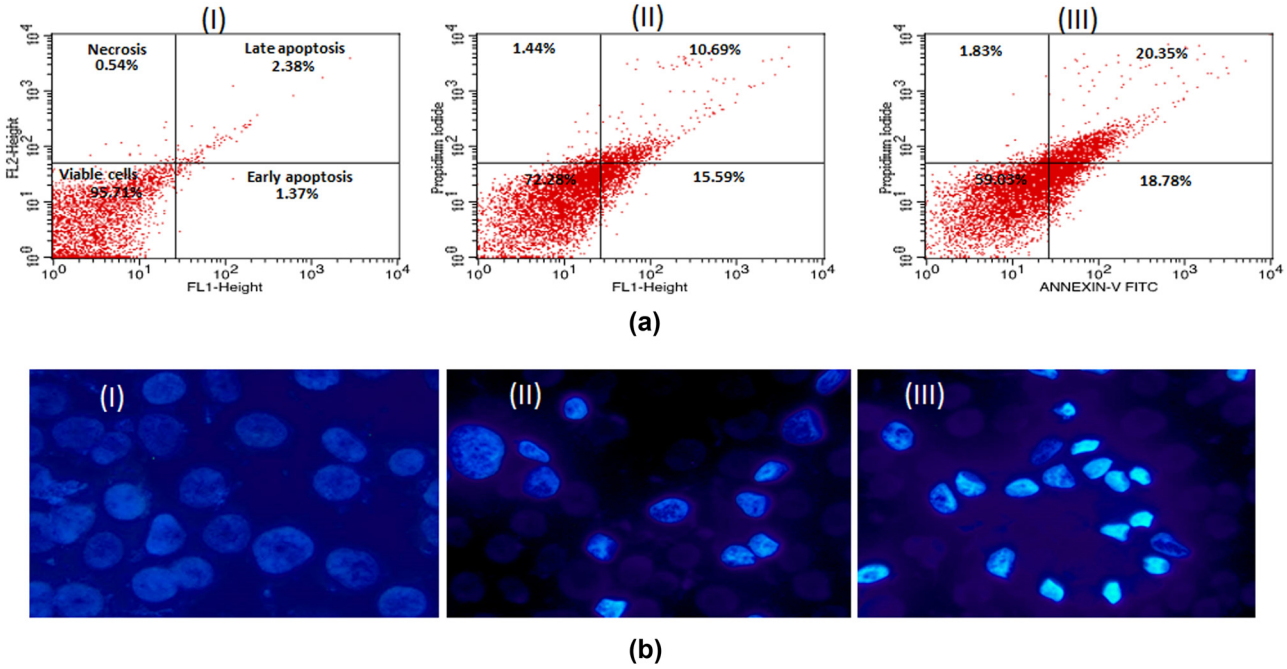

Figure 8: (a) Flow cytometry profile of annexin V-FITC/PI staining of MCF-7 cells showing percentage of viable cells, early apoptosis, late apoptosis, and necrotic cells. (I) Control, (II) 5 µg/mL of AuNPs, (III) 10 µg/mL of AuNPs. (b) Representative images of AuNPs-treated MCF-7 cells captured under fluorescence microscope after staining with nuclear dye Hoechst 33324. (I) Control, (II) 5 µg/mL, (III) 10 µg/mL. Magnification 200×.

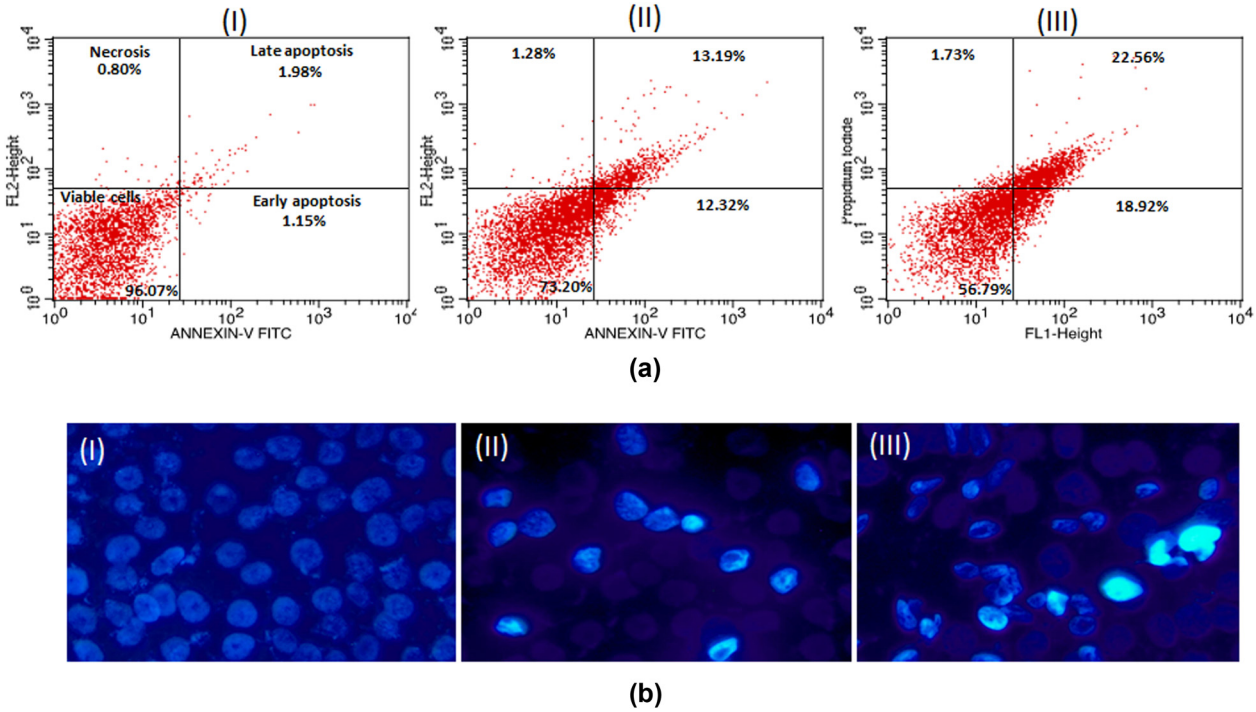

Figure 9: (a) Flow cytometry profile of annexin V-FITC/PI staining of HCT-116 cells showing percentage of viable cells, early apoptosis, late apoptosis and necrotic cells. (I) Control, (II) 5 µg/mL of AuNPs, (III) 10 µg/mL of AuNPs. (b) Representative images of AuNPs-treated HCT-116 cells captured under fluorescence microscope after staining with nuclear dye Hoechst 33324. (I) Control, (II) 5 µg/mL, (III) 10 µg/mL. Magnification 200×.

is frequently performed [49]. Exposure time, particle size, cell types, and NP surface coating significantly impact DNA damage [50]. A recent study reported that a positive surface charge increases the cellular absorption and cytotoxicity of AuNP. Neither functionalization nor size can result in genotoxicity [51]. However, one study reported a dose-dependent increase in DNA damage in HepG2 cells and suggested that the particle size of AuNPs affects their genotoxicity [39]. An earlier study reported that HepG2 cells are more susceptible to DNA damage by AuNPs than peripheral blood mononuclear cells, implying that specific cells are more sensitive to AuNPs cytotoxicity than others [52]. This could be explained because AuNPs affect physiological processes in different cell types through multiple signaling pathways [50]. We also observed genotoxicity/DNA damage in both the studied cancer cell lines due to AuNPs treatment.

A physiological system's redox state balance is required for proper biochemical functioning, and an imbalance creates oxidative stress, leading to pathogenic processes [53,54]. AuNPs' response to cellular ROS production is one of the primary factors of NP-induced cytotoxicity. The interaction of AuNPs and mammalian cells might cause oxidative stress by promoting ROS production over the cellular antioxidant defenses [55]. ROS production could also play a significant role in the apoptosis induced by AuNPs treatment [53]. AuNPs have also been shown to stimulate ROS generation in different cancer cell lines [53–55]. Our findings revealed a molecular basis of AuNPs-induced ROS production, leading to apoptosis. These findings also suggest that the cell death observed in our study could be due to ROS generation, which may have disturbed the cellular redox balance.

p53 encourages cell arrest in the presence of DNA damage or cellular stress so that the damage can be repaired, or self-mediated apoptosis can take place [17,56]. The activated caspases-3 are capable of autocatalysis, cleaving, and activating other caspase family members, culminating in irreversible apoptosis [57]. Our study also observed DNA fragmentation and increased caspase-3 activity in MCF-7 and HCT-116 cancer cells treated with AuNPs. Apoptosis is crucial for many biological processes and systems, including the immune system, the normal cell cycle, anticancer defenses, embryonic development, morphological changes, and chemically induced cell death [58]. Our findings are in accordance with the previous reports by Kim *et al.* [59] and Ahmadian *et al.* [60]. Given the specific apoptotic response in cancer cells, the RT-PCR results also revealed a modulation in expression levels of the studied pro/anti-apoptotic proteins in both cancer cell lines, confirming the anticancer potential of our synthesized AuNPs.

5 Conclusion

In summary, the current study observed the diverse impacts of synthesized AuNPs on human cancer cell (HCT-116 and MCF-7) viability. The considerable difference in AuNP-induced cytotoxicity in cancer cells highlights that it could be a viable alternative to more harmful traditional cancer therapies. The AuNPs trigger apoptosis in cancer cells *via* the ROS-regulated p53, Bax/Bcl-2, and caspase pathways. However, more in-depth research is needed to understand the exact mechanism resulting from AuNPs' cancer cell-specific toxicity, which is still mostly unknown.

Funding information: The authors extend their appreciation to the Deputyship for Research & Innovation, Ministry of Education in Saudi Arabia for funding this research work through the project no. (IFKSURG-2-1734).

Author contributions: All authors have accepted responsibility for the entire content of this manuscript and approved its submission.

Conflict of interest: The authors state no conflict of interest.

References

[1] Pradhan RK, Ramakrishna W. Transposons: Unexpected players in cancer. Gene. 2022;808:145975.
[2] Khan MS, Alomari A, Tabrez S, Hassan I, Wahab R, Bhat SA, et al. Anticancer potential of biogenic silver nanoparticles: A mechanistic study. Pharmaceutics. 2021;13(5):707.
[3] Zughaibi TA, Suhail M, Tarique M, Tabrez S. Targeting PI3K/Akt/mTOR pathway by different flavonoids: A cancer chemopreventive approach. Int J Mol Sci. 2021;22(22):12455.
[4] Hadhri A, Abidi R, Mahjoub N, Mousli A, Mahjoubi K, Boujelbene N, et al. Metastasis of breast cancer to bladder. Afr J Urol. 2021;27(1):123.
[5] Łukasiewicz S, Czeczelewski M, Forma A, Baj J, Sitarz R, Stanisławek A. Breast cancer epidemiology, risk factors, classification, prognostic markers, and current treatment strategies-an updated review. Cancers. 2021;13(17):4287.
[6] Veettil SK, Wong TY, Loo YS, Playdon MC, Lai NM, Giovannucci EL, et al. Role of diet in colorectal cancer incidence: Umbrella review of meta-analyses of prospective observational studies. JAMA Netw Open. 2021;4(2):e2037341.

[7] Tabrez S, Khan AU, Mirza AA, Suhail M, Jabir NR, Zughaibi TA, et al. Biosynthesis of copper oxide nanoparticles and its therapeutic efficacy against colon cancer. Nanotechnol Rev. 2022;11(1):1322–31.
[8] Cheng Z, Li M, Dey R, Chen Y. Nanomaterials for cancer therapy: current progress and perspectives. J Hematol Oncol. 2021;14(1):85.
[9] Kemp JA, Kwon YJ. Cancer nanotechnology: current status and perspectives. Nano Convergence. 2021;8(1):34.
[10] Alserihi RF, Mohammed MRS, Kaleem M, Khan MI, Sechi M, Sanna V, et al. Development of (−)-epigallocatechin-3-gallate-loaded folate receptor-targeted nanoparticles for prostate cancer treatment. Nanotechnol Rev. 2022;11(1):298–311.
[11] Tabrez S, Jabir NR, Adhami VM, Khan MI, Moulay M, Kamal MA, et al. Nanoencapsulated dietary polyphenols for cancer prevention and treatment: successes and challenges. Nanomed (Lond). 2020;15(11):1147–62.
[12] Tabrez S, Khan AU, Hoque M, Suhail M, Khan MI, Zughaibi TA. Investigating the anticancer efficacy of biogenic synthesized MgONPs: An *in vitro* analysis. Front Chem. 2022;10:970193.
[13] Mitchell MJ, Billingsley MM, Haley RM, Wechsler ME, Peppas NA, Langer R. Engineering precision nanoparticles for drug delivery. Nat Rev Drug Discov. 2021;20(2):101–24.
[14] Shait Mohammed MR, Ahmad V, Ahmad A, Tabrez S, Choudhry H, Zamzami MA, et al. Prospective of nanoscale metal organic frameworks [NMOFs] for cancer therapy. Semin Cancer Biol. 2021;69:129–39.
[15] Gerosa C, Crisponi G, Nurchi VM, Saba L, Cappai R, Cau F, et al. Gold nanoparticles: A new golden era in oncology? Pharmaceuticals. 2020;13(8):192.
[16] Saeed BA, Lim V, Yusof NA, Khor KZ, Rahman HS, Samad NA. Antiangiogenic properties of nanoparticles: a systematic review. Int J Nanomed. 2019;14:5135–46.
[17] Tabrez S, Khan AU, Hoque M, Suhail M, Khan MI, Zughaibi TA. Biosynthesis of ZnO N.P.s from pumpkin seeds' extract and elucidation of its anticancer potential against breast cancer. Nanotechnol Rev. 2022;11(1):2714–25.
[18] Elahi N, Kamali M, Baghersad MH. Recent biomedical applications of gold nanoparticles: A review. Talanta. 2018;184:537–56.
[19] Hu X, Zhang Y, Ding T, Liu J, Zhao H. Multifunctional gold nanoparticles: A novel nanomaterial for various medical applications and biological activities. Front Bioeng Biotechnol. 2020;8:990.
[20] Albarwary SA, Kibarer AG, Mustapha MT, Hamdan H, Ozsahin DU. The efficiency of AuNPs in cancer cell targeting compared to other nanomedicine technologies using fuzzy PROMETHEE. J Healthc Eng. 2021;2021:e1566834.
[21] Bai X, Wang Y, Song Z, Feng Y, Chen Y, Zhang D, et al. The basic properties of gold nanoparticles and their applications in tumor diagnosis and treatment. Int J Mol Sci. 2020;21(7):E2480.
[22] Siddique S, Chow JCL. Gold nanoparticles for drug delivery and cancer therapy. Appl Sci. 2020;10(11):3824.
[23] Lu H, Su J, Mamdooh R, Li Y, Stenzel MH. Cellular uptake of gold nanoparticles and their movement in 3D multicellular tumor spheroids: Effect of molecular weight and grafting density of poly(2-hydroxyl ethyl acrylate). Macromol Biosci. 2020;20(1):1900221.
[24] Zhang X-D, Wu D, Shen X, Liu P-X, Yang N, Zhao B, et al. Size-dependent *in vivo* toxicity of PEG-coated gold nanoparticles. Int J Nanomed. 2011;6:2071–81.
[25] Adnan M, Oh K-K, Husen A, Wang M-H, Alle M, Cho D-H. Microwave-assisted synchronous nanogold synthesis reinforced by kenaf seed and decoding their biocompatibility and anticancer activity. Pharmaceuticals. 2022;15(2):111.
[26] Ali MRK, Wu Y, Ghosh D, Do BH, Chen K, Dawson MR, et al. Nuclear membrane-targeted gold nanoparticles inhibit cancer cell migration and invasion. ACS Nano. 2017;11(4):3716–26.
[27] Priya K, Iyer PR. Antiproliferative effects on tumor cells of the synthesized gold nanoparticles against Hep2 liver cancer cell line. Egypt Liver J. 2020;10(1):15.
[28] Alharthy SA, Tabrez S, Mirza AA, Zughaibi TA, Firoz CK, Dutta M. Sugiol suppresses the proliferation of human U87 glioma cells *via* induction of apoptosis and cell cycle arrest. Evid Based Complement Altern Med. 2022;2022:7658899.
[29] Hassan I, Khan AA, Aman S, Qamar W, Ebaid H, Al-Tamimi J, et al. Restrained management of copper level enhances the antineoplastic activity of imatinib *in vitro* and *in vivo*. Sci Rep. 2018;8(1):1682.
[30] Jabir NR, Khan MS, Alafaleq NO, Naz H, Ahmed BA. Anticancer potential of yohimbine in drug-resistant oral cancer KB-ChR-8-5 cells. Mol Biol Rep. 2022;49:9565–73.
[31] Hailan WA, Al-Anazi KM, Farah MA, Ali MA, Al-Kawmani AA, Abou-Tarboush FM. Reactive oxygen species-mediated cytotoxicity in liver carcinoma cells induced by silver nanoparticles biosynthesized using Schinus molle extract. Nanomaterials (Basel, Switz). 2022;12(1):161.
[32] Link S, El-Sayed MA. Size and temperature dependence of the plasmon absorption of colloidal gold nanoparticles. J Phys Chem B. 1999;103(21):4212–7.
[33] Mohanpuria P, Rana NK, Yadav SK. Biosynthesis of nanoparticles: technological concepts and future applications. J Nanopart Res. 2008;10(3):507–17.
[34] Yetisgin AA, Cetinel S, Zuvin M, Kosar A, Kutlu O. Therapeutic nanoparticles and their targeted delivery applications. Molecules (Basel, Switz). 2020;25(9):E2193.
[35] Jabir NR, Firoz CK, Bhushan A, Tabrez S, Kamal MA. The use of azoles containing natural products in cancer prevention and treatment: An overview. Anticancer Agents Med Chem. 2018;18(1):6–14.
[36] Ullah F, Shah KU, Shah SU, Nawaz A, Nawaz T, Khan KA, et al. Synthesis, characterization and *in vitro* evaluation of chitosan nanoparticles physically admixed with lactose microspheres for pulmonary delivery of montelukast. Polym (Basel). 2022;14(17):3564.
[37] Nguyen VP, Le Trung H, Nguyen TH, Hoang D, Tran TH. Advancement of microwave-assisted biosynthesis for preparing Au nanoparticles using Ganoderma lucidum extract and evaluation of their catalytic reduction of 4-Nitrophenol. ACS Omega. 2021;6(47):32198–207.
[38] Perveen K, Husain FM, Qais FA, Khan A, Razak S, Afsar T, et al. Microwave-assisted rapid green synthesis of gold nanoparticles using seed extract of Trachyspermum ammi: ROS mediated biofilm inhibition and anticancer activity. Biomolecules. 2021;11(2):197.
[39] Xia Q, Li H, Liu Y, Zhang S, Feng Q, Xiao K. The effect of particle size on the genotoxicity of gold nanoparticles. J Biomed Mater Res A. 2017;105(3):710–9.

[40] Zhang X-D, Wu D, Shen X, Liu P-X, Fan F-Y, Fan S-J. *In vivo* renal clearance, biodistribution, toxicity of gold nanoclusters. Biomaterials. 2012;33(18):4628–38.
[41] Vines JB, Yoon J-H, Ryu N-E, Lim D-J, Park H. Gold nanoparticles for photothermal cancer therapy. Front Chem. 2019;7:167.
[42] Majoumouo MS, Sharma JR, Sibuyi NRS, Tincho MB, Boyom FF, Meyer M. Synthesis of biogenic gold nanoparticles from Terminalia mantaly extracts and the evaluation of their *in vitro* cytotoxic effects in cancer cells. Molecules. 2020;25(19):4469.
[43] Jeyarani S, Vinita NM, Puja P, Senthamilselvi S, Devan U, Velangani AJ, et al. Biomimetic gold nanoparticles for its cytotoxicity and biocompatibility evidenced by fluorescence-based assays in cancer (MDA-MB-231) and non-cancerous (HEK-293) cells. J Photochem Photobiol B: Biol. 2020;202:111715.
[44] Kus-Liśkiewicz M, Fickers P, Ben Tahar I. Biocompatibility and cytotoxicity of gold nanoparticles: recent advances in methodologies and regulations. Int J Mol Sci. 2021;22(20):10952.
[45] Peng J, Liang X. Progress in research on gold nanoparticles in cancer management. Med (Baltim). 2019;98(18):e15311.
[46] Liang C-C, Park AY, Guan J-L. *In vitro* scratch assay: a convenient and inexpensive method for analysis of cell migration *in vitro*. Nat Protoc. 2007;2(2):329–33.
[47] Hevia LG, Fanarraga ML. Microtubule cytoskeleton-disrupting activity of MWCNTs: applications in cancer treatment. J Nanobiotechnology. 2020;18(1):181.
[48] Zughaibi TA, Mirza AA, Suhail M, Jabir NR, Zaidi SK, Wasi S, et al. Evaluation of anticancer potential of biogenic copper oxide nanoparticles (CuO N.P.s) against breast cancer. J Nanomater. 2022;2022:5326355. doi: 10.1155/2022/5326355.
[49] Bankoglu EE, Schuele C, Stopper H. Cell survival after DNA damage in the comet assay. Arch Toxicol. 2021;95(12):3803–13.
[50] Wang Y, Zhang H, Shi L, Xu J, Duan G, Yang H. A focus on the genotoxicity of gold nanoparticles. Nanomedicine. 2020;15(4):319–23.
[51] Vales G, Suhonen S, Siivola KM, Savolainen KM, Catalán J, Norppa H. Genotoxicity and cytotoxicity of gold nanoparticles *in vitro*: role of surface functionalization and particle size. Nanomaterials. 2020;10(2):271.
[52] Paino IMM, Marangoni VS, de Oliveira RD, Antunes LMG, Zucolotto V. Cyto and genotoxicity of gold nanoparticles in human hepatocellular carcinoma and peripheral blood mononuclear cells. Toxicol Lett. 2012;215(2):119–25.
[53] Jawaid P, Rehman MU, Zhao Q-L, Misawa M, Ishikawa K, Hori M, et al. Small size gold nanoparticles enhance apoptosis induced by cold atmospheric plasma *via* depletion of intracellular GSH and modification of oxidative stress. Cell Death Discov. 2020;6(1):1–12.
[54] Sen GT, Ozkemahli G, Shahbazi R, Erkekoglu P, Ulubayram K, Kocer-Gumusel B. The effects of polymer coating of gold nanoparticles on oxidative stress and DNA damage. Int J Toxicol. 2020;39(4):328–40.
[55] Enea M, Pereira E, Peixoto de Almeida M, Araújo AM, Bastos MD, Carmo H. Gold nanoparticles induce oxidative stress and apoptosis in human kidney cells. Nanomaterials. 2020;10(5):995.
[56] Bieging KT, Mello SS, Attardi LD. Unravelling mechanisms of p53-mediated tumour suppression. Nat Rev Cancer. 2014;14(5):359–70.
[57] Araya LE, Soni IV, Hardy JA, Julien O. Deorphanizing Caspase-3 and Caspase-9 Substrates In and Out of Apoptosis with Deep Substrate Profiling. ACS Chem Biol. 2021;16(11):2280–96.
[58] Zhang Y, Li X, Huang Z, Zheng W, Fan C, Chen T. Enhancement of cell permeabilization apoptosis-inducing activity of selenium nanoparticles by ATP surface decoration. Nanomedicine. 2013;9(1):74–84.
[59] Kim S, Choi JE, Choi J, Chung K-H, Park K, Yi J, et al. Oxidative stress-dependent toxicity of silver nanoparticles in human hepatoma cells. Toxicol Vitro. 2009;23(6):1076–84.
[60] Ahmadian E, Dizaj SM, Rahimpour E, Hasanzadeh A, Eftekhari A, Hosain Zadegan H, et al. Effect of silver nanoparticles in the induction of apoptosis on human hepatocellular carcinoma (HepG2) cell line. Mater Sci Eng C Mater Biol Appl. 2018;93:465–71.